NO$_3$ chemistry of wildfire emissions: a kinetic study of the gas-phase reactions of furans with the NO$_3$ radical

Mike J. Newland, Yangang Ren, Max R. McGillen, Lisa Michelat, Véronique Daële, Abdelwahid Mellouki

ICARE-CNRS, 1 C Av. de la Recherche Scientifique, 45071 Orléans Cedex 2, France

Correspondence to: Mike J. Newland (mike.newland@cnrs-orleans.fr); Abdelwahid Mellouki (mellouki@cnrs-orleans.fr)

Abstract. Furans are emitted to the atmosphere during biomass burning from the pyrolysis of cellulose. They are one of the major contributing VOC classes to OH and NO$_3$ reactivity in biomass burning plumes. The major removal process of furans from the atmosphere at night is reaction with the nitrate radical, NO$_3$. Here we report a series of relative rate experiments in the 7300 L indoor simulation chamber at CNRS-ICARE, Orléans, using a number of different reference compounds to determine NO$_3$ reaction rate coefficients for four furans, two furanones, and pyrrole. In the case of the two furanones, this is the first time that NO$_3$ rate coefficients have been reported. The recommended values (cm^3 molecule^{-1} s^{-1}) are: furan $(1.49\pm0.23)\times10^{-12}$, 2-methylfuran $(2.26\pm0.52)\times10^{-11}$, 2,5-dimethylfuran $(1.02\pm0.31)\times10^{-10}$, furfural (furan-2-aldehyde) $(9.07\pm2.3)\times10^{-14}$, α-angelicalactone (5-methyl-2(3H)-furanone) $(3.01\pm0.45)\times10^{-12}$, γ-crotonolactone (2(5H)-furanone) $<1.4\times10^{-16}$, and pyrrole $(6.94\pm1.9)\times10^{-11}$. The furfural + NO$_3$ reaction rate coefficient is found to be an order of magnitude smaller than previously reported. These experiments show that for furan, alkyl substituted furans, α-angelicalactone, and pyrrole, reaction with NO$_3$ will be the dominant removal process at night, and may also contribute during the day. For γ-crotonolactone, reaction with NO$_3$ is not an important atmospheric sink.

1 Introduction

Furans are five membered aromatic cyclic ethers. Furans (and pyrroles – where N replaces O as the heteroatom) are generated during the pyrolysis of cellulose and are a major component of emissions from wildfire burning (Hatch et al., 2015, 2017; Koss et al., 2018; Coggon et al., 2019; Andreae et al., 2019). Such emissions are likely to increase in the future with the spatial extent, number, and severity, of wildfires globally having increased markedly in recent decades (Jolly et al., 2015; Harvey, 2016) and predicted to continue to do so as the climate warms (Krikken et al., 2019; Lohmander, 2020). Furans have also been measured in emissions from residential logwood burning (Hartikainen et al., 2018), and burning of a wide variety of solid-fuels used for domestic heating and cooking (Stewart et al., 2021a). Furans have been shown to account for a significant proportion of the total NO$_3$ (Decker et al., 2019) and OH (Koss et al., 2018; Coggon et al., 2019; Stewart et al., 2021b) reactivity of emissions from burning of typical wildfire and domestic fuels.

Alkyl substituted furans have also been suggested as promising biofuels as they can be derived from lignocellulosic biomass (Roman-Leshkov et al., 2007; Binder et al., 2009; Wang et al., 2014). This would likely lead to fugitive emissions of these compounds during distribution, as well as emissions of unburned and partially oxidised products from vehicle exhaust. The oxidation of certain furan compounds has been shown to have large secondary organic aerosol yields (Hatch et al., 2017; Hartikainen et al., 2018; Joo et al., 2019, Ahern et al., 2019; Akherati et al., 2020), which could adversely impact air quality.

Oxidation of furans in the atmosphere has been shown to produce 2-furanones (mono-unsaturated five-membered cyclic esters) both via OH (notably hydroxy-furan-2-ones, Aschmann et al., 2014) and NO$_3$ (Berndt et al., 1997) reactions. 2-Furanones are

38 also produced from the OH oxidation of six-membered aromatic compounds (Smith et al., 1998, 1999; Hamilton et al., 2005;
39 Bloss et al., 2005; Wyche et al., 2009; Huang et al., 2015). In both cases, the initial product is thought to be an unsaturated
40 dicarbonyl, with production of the 2-furanone formed via photoisomerisation of the dicarbonyl to a ketene-enol (Newland et al.,
41 2019), followed by ring closure of this molecule. In the case of aromatics, the ketene-enol can also be formed directly via
42 decomposition of the bicyclic peroxy radical intermediate (Wang et al., 2020).

43 Furan type compounds are removed from the atmosphere by reaction with the major oxidants OH, NO_3 and O_3. There have been
44 a number of studies on the rates of reaction of furan type compounds with the dominant daytime oxidant, OH (Lee and Tang,
45 1982; Atkinson et al., 1983; Wine and Thompson, 1984; Bierbach et al., 1992, 1994, 1995; Aschmann et al., 2011; Ausmeel et
46 al., 2017; Whelan et al., 2020). However, there have been fewer studies on the rates of reaction of furan type compounds with
47 the major night-time oxidant, NO_3 (Atkinson et al., 1985; Kind et al., 1996; Cabañas et al., 2004; Colmenar et al., 2012).

48 The nitrate radical, NO_3, is produced in the atmosphere predominantly through the reaction of NO_2 with O_3, and exists in
49 equilibrium with N_2O_5. It has long been known to be an important night-time oxidant (Levy, 1972; Winer et al., 1984). While it
50 is also produced during the daytime, it is rapidly converted back to NO_2 by reaction with NO and by photolysis. However, in
51 environments with low NO, either due to low NOx emissions, or suppression through high O_3 concentrations (e.g. Newland et
52 al., 2021), NO_3 oxidation has been observed to be significant during the day (Hamilton et al., 2021).

53 Here, we present results of a series of relative rate experiments for furan, 2-methylfuran, 2,5-dimethylfuran, furfural (furan-2-
54 aldehyde), α-angelicalactone (5-methyl-2(3H)-furanone), γ-crotonolactone (2(5H)-furanone), and pyrrole reaction with the NO_3
55 radical, performed in the 7300 L indoor simulation chamber at CNRS-ICARE, Orléans, France.

56 2 Experimental

57 2.1   CSA-Chamber

58
59 The CNRS-ICARE indoor chamber is a 7300 L indoor simulation chamber used for studying reaction kinetics and mechanisms
60 under atmospheric boundary layer conditions. Further details of the chamber setup and instrumentation are available elsewhere
61 (Zhou et al., 2017). Experiments were performed in the dark at atmospheric pressure (*ca.* 1000 mbar), with the chamber operated
62 at a slight overpressure to compensate for removal of air for sampling, and to prevent ingress of outside air to the chamber. The
63 chamber is in a climate controlled room and the temperature was maintained at 299±2 K.

64
65 2.2   Experimental Approach

66
67 Starting with the chamber filled with clean air, the VOCs of interest (*ca.* 3 ppmv) were added, followed by ~ 1 Torr of the inert
68 gas SF_6 to monitor the chamber dilution rate. A flow of 5 L/min of purified air was continuously added throughout the experiment,
69 and air is then removed from the chamber to maintain a constant pressure (this is a slight overpressure to prevent possible ingress
70 of air from outside the chamber). The chamber was left for at least thirty minutes prior to the start of the experiment to monitor
71 the dilution rate and losses of the VOCs to the chamber walls. These losses, $(1 - 8) \times 10^{-6} \, s^{-1}$, were always smaller than dilution
72 $(\sim 1.2 \times 10^{-5} \, s^{-1})$. The reaction was then initiated by continuously introducing an N_2O_5 sample, held in a trap at ~ 235 K with a part
73 of the purified air flow (2.5 – 5) L/min directed through it, for the duration of the experiment. The chamber was monitored until

75 most of the VOC of interest was consumed, with experiments generally taking 0.5 – 2 hours. The experiments were performed
76 under dry conditions (RH ≤ 1.5 %).
77 VOC abundance was determined by *in-situ* Fourier Transform Infrared (FTIR) Spectroscopy using a Nicolet 5700 coupled to a
78 White-type multipass cell with a pathlength of 143 m. Each scan was comprised of either 30 or 60 co-additions, taking a total of
79 2 or 4 minutes respectively, depending on the expected rate of loss of the VOCs, with a spectral resolution of 0.25 cm^{-1}.
80

81 **2.3   Materials**

82

83 The VOCs of interest: furan (>99%, Sigma-Aldrich), 2-methylfuran (>98%, TCI), 2,5-dimethylfuran (>98%, TCI), pyrrole
84 (>99%, TCI), α-angelicalactone (>98%, TCI), furfural (>98%, TCI), and γ-crotonolactone (>93%, TCI); and reference
85 compounds: 2,3-dimethyl-but-2-ene (98%, Sigma-Aldrich), 2-carene (97%, Sigma-Aldrich), camphene (95%, Sigma-Aldrich),
86 α-pinene (98%, Sigma-Aldrich), cyclohexene (≥99%, Sigma-Aldrich), 3-methyl-3-buten-1-ol (97%, Sigma-Aldrich), and
87 cyclohexane (99.5%, Sigma-Aldrich), were used as supplied without further purification.
88 N_2O_5 was synthesised by reacting NO_2 with excess O_3. First, NO and O_3 were mixed to generate NO_2 (Reaction R1). This NO_2 /
89 O_3 mixture was then flushed into a bulb in which NO_3 and subsequently N_2O_5 were generated through Reactions R2-R3.
90
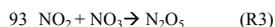
91 $NO + O_3 \rightarrow NO_2$ (R1)
92 $NO_2 + O_3 \rightarrow NO_3$ (R2)
93 $NO_2 + NO_3 \rightarrow N_2O_5$ (R3)
94

95 N_2O_5 crystals were then collected in a cold trap at 190K. The N_2O_5 sample was purified by trap to trap distillation under a flow
96 of O_2 / O_3. The final sample was stored at 190 K and used within a week.
97

98 **2.4   Analysis**

99

100 VOC concentrations were monitored by FTIR. The furans generally have a number of major absorption bands in the infrared.
101 The main bands used for analysis are shown in Table 1 (bold), as well as other characteristic bands for each compound. Reference
102 spectra of the major bands for each compound taken in the chamber at a resolution of 0.25 cm^{-1} are provided in the Supplement
103 (Figures S8-S14). The ANIR curve fitting software (Ródenas, 2018), which implements a least squares fitting algorithm was
104 used to generate time profiles for each compound based on their reference spectra. Profiles were checked by doing a number of
105 manual subtractions. Example time profiles from an experiment with α-angelicalactone and furan, with cyclohexene as the
106 reference compound, are shown in Figure 1. Further example plots are provided in the supplement (Figures S1-S7). All of the
107 concentration-time profiles are provided in .txt format at 10.5281/zenodo.5721518, and all the raw FTIR output is provided in
108 .csv format at 10.5281/zenodo.5721518. Relative rate plots for all of the experiments are shown in Figure 2.
109
110
111
112
113

115

116

Table 1 Maxima of major absorption bands (of Q branches if present) for the compounds used in this study. Bands used predominantly for analysis are shown in bold.

Compound	Main absorption bands / cm^{-1}
Furan	**995**, 744
2-Methylfuran	**792**, 726, 1151, 2965
2,5-Dimethylfuran	**777**, 2938, 2961
Furfural	**756**, 1720
Pyrrole	**724**, 1017, 3531, 718-722
α-angelicalactone	**731, 939**, 1100, 1834
γ-crotonolactone	**1098,** 805, 866, 1045, 1812, 2885, 2945
2,3-Dimethyl-2-butene	**2878, 2930, 3005**
2-Carene	**2874, 2928, 3009**
α-pinene	**2971, 2998, 3035,** 789, 2847, 2893, 2925, 2931
Camphene	**2967, 2972, 2986**, 882, 2881, 3075
Cyclohexene	**2934,** 744, 919, 1140, 2892, 2943, 3033, 3036
3-Methyl-3-buten-1-ol	**1065,** 896, 903, 2886, 2948, 2981, 3084
Cyclohexane	**2862, 2933**

119

120 Relative rate experiments were performed, whereby a compound (or two) with an unknown reaction rate coefficient (k_{VOC}) with

121 NO$_3$ was added to the chamber with a reference compound with a known NO$_3$ reaction rate coefficient (k_{ref}). A plot of the relative

122 loss of the compound against the reference compound following addition of NO$_3$ (via N$_2$O$_5$ decomposition), accounting for both

123 chamber dilution and wall losses (k_d), gives a gradient of k_{VOC}/k_{ref} (Equation E1).

124

125 $$\ln\frac{([VOC]_0)}{([VOC]_t)} - k_d t = \frac{k_{VOC}}{k_{ref}}\ln\frac{[ref]_0}{[ref]_t} - k_d t \qquad (E1)$$

126

127 A number of reference compounds were used for each VOC, chosen so that the reference rate coefficient was roughly within a

128 factor of five of the expected unknown rate coefficient, and with an attempt to use different references that had both larger and

129 smaller NO$_3$ reaction rate coefficients than the VOC. Rate coefficients of the reference compounds (Table 2) are taken from the

130 Database for the Kinetics of the Gas-Phase Atmospheric Reactions of Organic Compounds v2.1.0 (McGillen et al., 2020),

131 available at data.eurochamp.org/data-access/kin/#/home.

132 N$_2$O$_5$ was not present at detectable levels (by FTIR) during most of the experiments. The only experiments in which N$_2$O$_5$

133 concentrations built up in the chamber, were those with the slowest reacting VOCs, i.e. furfural and γ-crotonolactone. NO$_2$

134 concentrations increased throughout all experiments, typically up to 2 – 3 ppmv. The NO$_2$ is initially produced from the

135 decomposition of N$_2$O$_5$, and later potentially by the loss of NO$_2$ from nitrated VOCs / nitrated radicals. HNO$_3$ concentrations

136 increased throughout the experiments, typically up to 3 – 4 ppmv. This could be either due to impurities in the N_2O_5 sample, or
137 from H abstraction reactions of NO_3. It is not thought that this level of HNO_3 will cause any interference in the rate coefficient
138 determinations.
139
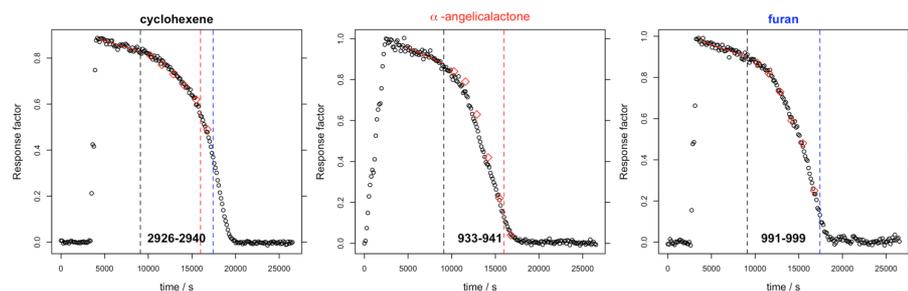
140
141 **Figure 1** Concentration-time profiles from experiment with cyclohexene, α-angelicalactone and furan. Black circles are response
142 factors generated by the ANIR curve fitting program relative to the reference spectra. Red diamonds are obtained from manual
143 subtractions. Left black dashed vertical line is the beginning of the region used for the relative rate calculation, the red dashed
144 line is the end of the region used for the calculation of the α-angelicalactone relative rate, the blue line is the end of the region
145 used for the calculation of the furan relative rate. Bold values at the bottom are the absorption bands used for analysis.

146 **Table 2.** Reference compounds used. Recommended rate coefficients and uncertainties from McGillen et al. (2020).

Compound	k / cm^3 molecule^{-1} s^{-1}
2,3-dimethyl-2-butene	$(5.70\pm1.71)\times10^{-11}$
2-carene	$(2.0\pm0.3)\times10^{-11}$
α-pinene	$(6.20\pm1.55)\times10^{-12}$
camphene	$(6.60\pm1.65)\times10^{-13}$
cyclohexene	$(5.60\pm0.84)\times10^{-13}$
3-methyl-3-buten-1-ol	$(2.60\pm0.78)\times10^{-13}$
cyclohexane	$(1.35\pm0.20)\times10^{-16}$

147
148 It is noted that no OH scavenger was used in these experiments (as is the case for most, if not all, NO_3 previous relative rate
149 studies to the authors' knowledge). NO_3 reaction with alkenes tends to proceed by electrophilic addition to the double bond
150 followed by addition of O_2 to the resulting radical, leading to a nitrooxy peroxy radical (β-ONO_2-RO_2) (Barnes et al., 1989;
151 Hjorth et al., 1990). It has recently been shown (Novelli et al., 2021) that there is the possibility of OH formation through the
152 reactions of β-ONO_2-RO_2 with HO_2. HO_2 could be generated in these experiments from the abstraction of an H atom by O_2 from
153 a β-ONO_2-RO radical with available H atoms. The initial NO_3 reaction with furans is not thought to form β-ONO_2-RO_2 radicals,
154 with NO_3 addition to the C2 carbon followed by O_2 addition to the C_5 carbon (Berndt et al., 1997), analogous to the OH addition
155 reaction (Bierbach et al., 1995; Mousavipour et al., 2009; Yuan et al., 2017; Whelan et al., 2020). However, some of the reference
156 compounds used in the experiments will form such radicals. For example, the reaction of HO_2 with the β-ONO_2-RO_2 radicals

157 formed from α-pinene + NO$_3$ has been reported to have an OH yield of up to 70 % (Kurtén et al., 2017). An additional minor
158 source of HO$_2$ during the experiments will be H abstraction reactions by NO$_3$. These will produce RO$_2$ that can react to form RO
159 radicals which may yield HO$_2$ following abstraction of an H atom by O$_2$. However, the rate coefficient of H abstraction by NO$_3$
160 is generally expected to be negligible relative to that of the NO$_3$ addition pathway. A box model run was performed to test the
161 impact of this chemistry in this study. The α-pinene scheme from the MCMv3.3.1 (Jenkin et al., 1997; mcm.york.ac.uk) was
162 incorporated into the box model AtChem (Sommariva et al., 2020), and an OH yield of 0.5 was assigned to the reaction of HO$_2$
163 with the initial β-ONO$_2$-RO$_2$ radicals formed from the α-pinene+NO$_3$ reaction. The model was initiated with 2-methylfuran and
164 α-pinene concentrations of 3 ppmv, representative of the experiments performed here. NO$_3$ concentrations were constrained to
165 give a lifetime of ~ 1 hour for the VOCs, typical of the experiments. OH reaction was found to account for less than 1 % of the
166 removal of 2-methylfuran or α-pinene through the model run. Consequently, it can be assumed that OH chemistry is a negligible
167 interference in these experiments.
168 A further potential interference with the current experimental setup, is the reaction of NO$_2$ with the compounds used. Rate
169 coefficients have been measured for reaction of NO$_2$ with a number of unsaturated compounds (Atkinson et al., 1984; Bernard
170 et al., 2013). For conjugated dienes, these values can be large enough (~10^{-18} cm^3 molecule^{-1} s^{-1}) to provide a significant loss
171 under the experimental conditions employed here, NO$_2$ is formed during these experiments from the decomposition of N$_2$O$_5$,
172 with the NO$_2$ mixing ratio typically increasing up to roughly 3 ppmv through the experiment. Separate experiments were
173 performed to look at the potential reaction of NO$_2$ with furan, 2,5-dimethylfuran and pyrrole. The experiments were performed
174 with initial VOC mixing ratios of 3 ppmv, and initial NO$_2$ mixing ratios of roughly 5 ppmv, similar to the maximum amount of
175 NO$_2$ observed during the NO$_3$ experiments. For all three compounds, their loss in the presence of NO$_2$ (allowing for dilution)
176 was indistinguishable from zero, allowing an upper limit of < 2×10^{-20} cm^3 molecule^{-1} s^{-1} to be placed on their k(NO$_2$) rate
177 coefficients. Based on these experiments, it was assumed that the k(NO$_2$) rate coefficients for 2-methylfuran, furfural, and a-
178 angelicalactone are likely to be of a similar magnitude, and hence provide negligible interference under the experimental
179 conditions employed.
180
181

| Moved (insertion) [1] |

Moved up [1]: (Atkinson et al., 1984; Bernard et al., 2013)

183
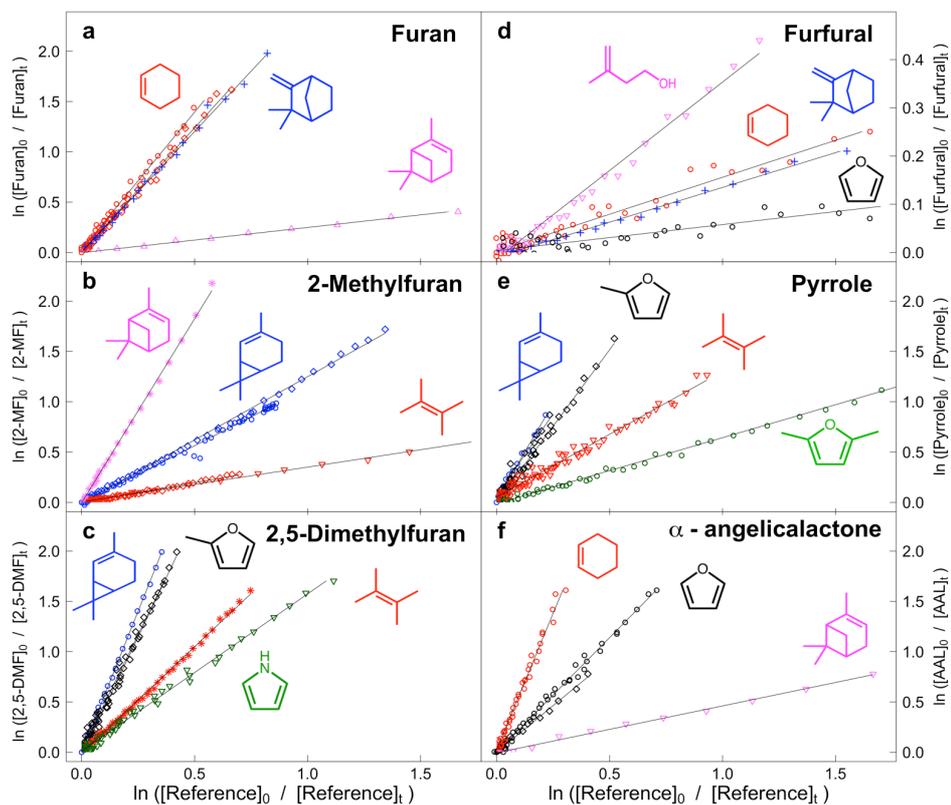
Figure 2. Relative rate plots for: **a.** furan relative to cyclohexene (red), camphene (blue), and α-pinene (pink); **b.** 2-methylfuran relative to 2-carene (blue), 2,3-dimethyl-2-butene (red), and α-pinene (pink); **c.** 2,5-dimethylfuran relative to 2-carene (blue), 2,3-dimethyl-2-butene (red), 2-methylfuran (black), and pyrrole (green); **d.** furfural relative to camphene (blue), cyclohexene (red), furan (black), and 3-methyl-3-buten-1-ol (pink); **e.** pyrrole relative to 2-carene (blue), 2,3-dimethyl-2-butene (red), 2-methylfuran (black), and 2,5-dimethylfuran (green); **f.** α-angelicalactone relative to cyclohexene (red), furan (black), and α-pinene (pink). Different shapes are used for different experiments with the same reference compound.

3 Results and Discussion

The $k(NO_3)$ rate coefficients determined with each reference compound are given in Table 3 and Figure 3. Overall recommended values for the rate coefficient for each compound are calculated by taking the mean (weighted by the reported uncertainty of the reference) of the rate coefficient derived from each experiment with each reference compound, including using the recommended values for the other furans presented in Table 3. Uncertainties for the relative rates in Table S1 are assumed to be < 10 % and to

---

197 be dominated by statistical errors in fitting to the absorption bands. Uncertainties for the rate coefficients reported in Table 3 are

198 dominated by the assumed uncertainties in $k(NO_3)$ of the reference compounds. For most of the references, the uncertainties are

199 20 – 30 %, taken from the recommendations of McGillen et al. (2020). For 2,3-dimethyl-2-butene, the recommended uncertainty

200 in McGillen et al. (2020) is 150 %, but based on the fact that the rate coefficients derived using 2,3-dimethyl-2-butene for 2-

201 methylfuran, 2,5-dimethylfuran and pyrrole agree very well with those using other references with much smaller uncertainties,

202 a conservative estimate of 30 % is used here. It is noted that for all compounds, the rate coefficients derived with different

203 references agree very well, to within 10%. The experimentally determined $k(NO_3)$ rate coefficients of the furans relative to each

204 other are in good agreement (to within 6%) with those calculated using the weighted means shown in Table 3 (Table S2). This

205 gives further confidence in the $k(NO_3)$ values used for the reference compounds.

206

207 The rate coefficient derived for furan, agrees well with the value previously reported by Atkinson et al. (1985) from a chamber

208 relative rate experiment. However, there is significant differences between the values reported here for furan, 2-methylfuran and

209 2,5-dimethylfuran, and those reported by Kind et al. (1996) from relative rate experiments in a flow reactor. While the value

210 reported for 2-methylfuran agrees within the uncertainties between the two studies, the values for furan and 2,5-dimethylfuran

211 reported here are ~ 50 % and 100 % greater respectively. It is unclear what is behind this observed disparity; the good agreement

212 between the two studies for the 2-methylfuran rate coefficient suggests that there is not a systematic difference between the

213 experimental setups. For pyrrole, the rate coefficient determined here is about 50% faster than the value reported by Atkinson et

214 al. (1985) from a chamber relative rate experiment using N_2O_5 thermal decomposition. Cabañas et al. (2004) reported an upper

215 limit of $<1.8\times10^{-10}$ cm^3 molecule^{-1} s^{-1} (298K) using an absolute technique of fast flow discharge.

216 For 2-furanaldehyde (furfural) + NO_3, the rate coefficient recommended here is an order of magnitude slower than the only

217 previously reported values (Colmenar et al., 2012), derived from small chamber relative rate experiments with 2-methyl-2-butene

218 and α-pinene as references. The rate coefficient from Colmenar et al. (2012) is very similar to the reported rate coefficient for

219 furan+NO_3. This is surprising, since the presence of a formyl group attached to a double bond is expected to be strongly

220 deactivating with respect to addition to that bond, due to the electron withdrawing mesomeric effect of the –C(O)H group

221 (Kerdouci et al., 2014). This has also been observed for other electrophilic addition reactions, such as those with OH and O_3

222 (Kwok and Atkinson, 1995; McGillen et al, 2011; Jenkin et al., 2020). And while there is the possibility of H abstraction from

223 the formyl group, which would increase the overall rate coefficient, such reactions are typically of the order of 10^{-14} cm^{3}s^{-1}

224 (Kerdouci et al., 2014), and hence would not be expected to compensate for the reduction in the contribution to the overall rate

225 coefficient of the addition reaction.

226 For 5-methyl-(3H)-furan-2-one (α-angelica lactone) + NO_3 this is the first reported rate coefficient. For (5H)-furan-2-one (γ-

227 crotonolactone), relative rate experiments with several reference compounds were attempted, with the slowest reacting of these

228 being cyclohexane ($k_{NO3} = 1.4\times10^{-16}$ cm^3 molecule^{-1} s^{-1}). In this experiment, roughly 10 % of the cyclohexane was removed by

229 reaction with NO_3 (accounting for loss by dilution), whereas there was no appreciable chemical loss of γ-crotonolactone. We can

230 therefore deduce that $k(\text{γ-crotonolactone}+NO_3) \ll 1.4\times10^{-16}$ cm^3 molecule^{-1} s^{-1}. Again, this is the first time a NO_3 reaction rate

231 coefficient has been measured for this compound. A comparison of the two furanones shows that 5-methyl-(3H)-furan-2-one

232 reacts more than four orders of magnitude faster than (5H)-furan-2-one. This can be explained in part by the presence of a methyl

233 group, which is seen to increase the rate coefficient by roughly an order of magnitude from e.g. furan to 2-methylfuran to 2,5-

234 dimethylfuran. Berndt et al. (1997) derived an NO_3 reaction rate coefficient of 1.76×10^{-13} cm^3 molecule^{-1} s^{-1} for (3H)-furan-2-

one. However, the majority of the difference must be explained by the structure of the two compounds, namely the conjugated nature of the C=C and C=O bonds in (5H)-furan-2-one. The carbonyl group removes electron density from the C=C bond greatly reducing the rate coefficient. A similar relationship is seen for analogous acyclic compounds e.g. the NO_3 rate coefficient of the conjugated ester methyl acrylate is almost two orders of magnitude greater than that of the non-conjugated isomer vinyl acetate.

Table 3. NO_3 reaction rate coefficients derived for each experiment and recommended value based on the weighted mean.

Compound	Reference (repeats)	$k(NO_3)$ / cm^3 molecule^{-1} s^{-1}	Weighted mean $k(NO_3)$ / cm^3 molecule^{-1} s^{-1}
2,5-dimethylfuran	2-carene (1)	1.12×10^{-10}	$1.02 \pm 0.31 \times 10^{-10}$
	2,3-dimethyl-2-butene (1)	1.21×10^{-10}	
	pyrrole (1)	9.12×10^{-11}	
	2-methylfuran (2)	9.06×10^{-11}	
pyrrole	2-carene (1)	7.68×10^{-11}	$6.94 \pm 1.9 \times 10^{-11}$
	2,3-dimethyl-2-butene (2)	7.07×10^{-11}	
	2,5-dimethylfuran (1)	6.58×10^{-11}	
	2-methylfuran (2)	6.37×10^{-11}	
2-methylfuran	2-carene (3)	2.47×10^{-11}	$2.26 \pm 0.52 \times 10^{-11}$
	2,3-dimethyl-2-butene (2)	2.12×10^{-11}	
	α-pinene (1)	2.27×10^{-11}	
	pyrrole (2)	1.89×10^{-11}	
	2,5-dimethylfuran (2)	2.21×10^{-11}	
α-angelicalactone	α-pinene (1)	2.89×10^{-12}	$3.01 \pm 0.45 \times 10^{-12}$
	cyclohexene (1)	3.03×10^{-12}	
	furan (2)	3.05×10^{-12}	
furan	cyclohexene (1)	1.45×10^{-12}	$1.49 \pm 0.23 \times 10^{-12}$
	α-pinene (1)	1.55×10^{-12}	
	camphene (1)	1.58×10^{-12}	
	α-angelicalactone (2)	1.49×10^{-12}	
furfural	cyclohexene (1)	8.57×10^{-14}	$9.07 \pm 2.30 \times 10^{-14}$
	3-methyl-3-buten-1-ol (1)	9.54×10^{-14}	
	furan	8.37×10^{-14}	
	camphene (1)	9.50×10^{-14}	
γ-crotonolactone	cyclohexane (1)	$< 1.4 \times 10^{-16}$	$< 1.4 \times 10^{-16}$

Deleted: ⁰
Deleted: ⁰
Deleted: C
Deleted: C
Deleted: C
Deleted: C
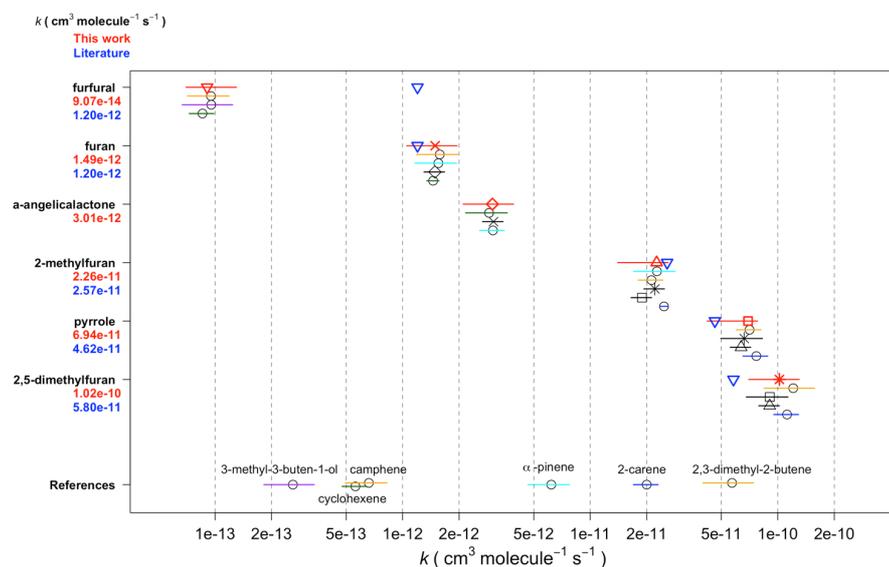
254

255 **Figure 3** The reaction rate coefficients derived for the six compounds in this work (excluding γ-crotonolactone). Red triangles
256 (and red text, left axis) represent the weighted mean of all experiments in this work, blue inverted triangles (and blue text, left
257 axis) are the recommended values from McGillen et al. (2020). Horizontal lines represent uncertainty in rate coefficient, colours
258 (shapes if other furans) represent which reference was used.

259

260

261 **Table 4.** Recommended NO_3 rate coefficients from this work compared to those reported in the literature.

Compound	Rate coefficient / cm^3 molecule^{-1} s^{-1}	Reference	Technique	NO_3 source
2,5-dimethylfuran	**(1.02±0.31)×10^{-10}**	**This work**		
	(5.78±0.34)×10^{-11}	Kind et al. (1996)	Flow reactor: relative (*trans*-2-butene)	N_2O_5
pyrrole	**(6.94±1.9)×10^{-11}**	**This work**		
	(4.6±1.1)×10^{-11}	Atkinson et al. (1985)	Chamber: relative (2-methyl-2-butene)	N_2O_5
	< 1×10^{-10}	Cabañas et al. (2004)	Flow reactor: absolute (LIF detection of NO_3)	HNO_3+F
2-methylfuran	**(2.26±0.52)×10^{-11}**	**This work**		
	(2.57±0.17)×10^{-11}	Kind et al. (1996)	Flow reactor: relative (*trans*-2-butene)	N_2O_5
α-angelicalactone	**(3.01±0.45)×10^{-12}**	**This work**		
furan	**(1.49±0.23)×10^{-12}**	**This work**		
	(1.5±0.2)×10^{-12} [b]	Atkinson et al. (1985)	Chamber: relative (*trans*-2-butene)	N_2O_5
	(0.998±0.062)×10^{-12}	Kind et al. (1996)	Flow reactor: relative (*trans*-2-butene)	N_2O_5
	(1.36±0.8)×10^{-12}	Cabañas et al. (2004)	Flow reactor: absolute (LIF detection of NO_3)	HNO_3+F

furfural	$(9.07\pm2.30)\times10^{-14}$	**This work**		
	$(1.17\pm0.15)\times10^{-12}$	Colmenar et al. (2012)	Small chamber: relative (2-methyl-2-butene)	N_2O_5
	$(1.36\pm0.38)\times10^{-12}$	Colmenar et al. (2012)	Small chamber: relative (α-pinene)	N_2O_5
γ-crotonolactone	$< 1.4\times10^{-16}$	**This work**		

262 [a] corrected for change to recommended rate for reference (2,3-dimethyl-2-butene); [b] corrected for change to recommended rate
263 for reference (trans-2-butene)

264

4 Atmospheric implications

266 The atmospheric lifetimes of the compounds, based on the rate coefficients reported herein, are given in Table 5. These assume
267 concentrations of OH = 5×10^6 molecules cm^{-3} (typical daily peak summertime concentrations 1.5×10^6 – 1.5×10^7 molecules cm^{-3}
268 (Stone et al., 2012)), night-time NO$_3$ = 2×10^8 molecules cm^{-3} (typical night-time concentrations 1×10^8 – $>1\times10^9$ cm^{-3} (Brown
269 and Stutz (2012)) daytime NO$_3$ = 1×10^7 molecules cm^{-3} (limited daytime measurements suggest concentrations ~ 0.5 – >1 pptv
270 (2.5×10^7 molecules cm^{-3}) (Brown and Stutz (2012)), and O$_3$ = 40 ppbv (background O$_3$ concentration ~ 40 ppb (Parrish et al.,
271 2014)). It is noted that oxidant concentrations have a high spatial and temporal variability due to variability in their sources and
272 sinks, and that oxidant levels within biomass burning plumes in particular are poorly understood. Hence the relative importance
273 of the oxidants shown in Table 5 is likely to vary dependent on conditions. From the values given in Table 5, it is clear that the

274 alkyl substituted furans and pyrrole have very short lifetimes both during the day, when the dominant daytime sink is likely to
275 be reaction with OH, and at night, when the dominant sink will be reaction with NO$_3$. O$_3$ may contribute somewhat to the removal
276 of these compounds both during the day and night, particularly for 2,5-dimethylfuran. As k(NO$_3$) approaches the same order of
277 magnitude as k(OH), e.g. for 2-methylfuran, 2,5-dimethylfuran and pyrrole, the NO$_3$ reaction is likely to be competitive with the
278 OH reaction even during the day in low NOx environments, with daytime NO$_3$ concentrations reported to be ~ 1 ppt (2.5×10^7
279 molecules cm^{-3}) (Brown and Stutz, 2012). The relatively large rate coefficient reported here for α-angelicalactone, suggests that
280 NO$_3$ reaction will be an important sink for unsaturated non-conjugated cyclic esters. On the other hand, the very small rate
281 coefficient for the γ-crotonolactone +NO$_3$ reaction suggests that this will not be an important atmospheric sink. γ-crotonolactone
282 has also been shown to have a very slow reaction with O$_3$ (lifetime > 100 years, Ausmeel et al., 2017), whereas for reaction with
283 OH, the lifetime is much shorter, and this will be the predominant gas-phase sink for γ-crotonolactone . Such a slow NO$_3$ reaction
284 might be expected to extend to all 2-furanones with a conjugated structure, e.g. hydroxyfuranones – major products of OH
285 oxidation of methyl substituted furans (Aschmann et al., 2014), such that the nitrate reaction may be unimportant in the
286 atmosphere for these structures. Although substitution at the double bond is likely to increase the rate coefficient somewhat, as
287 observed for OH and O$_3$ reactions with the methyl-substituted form of γ-crotonolactone (Ausmeel et al., 2017).
288 One of the major sources of furan type compounds to the atmosphere is wildfires. Wildfire plumes can be regions of high NO$_3$
289 even during the day due to suppressed photolysis rates in optically thick plumes (Decker et al, 2021). NO$_3$ oxidation of furans
290 may be even more important in such plumes than in the background atmosphere. Such plumes can extend over hundreds of
291 kilometres and hence affect air quality on a local and regional scale (e.g. Andreae et al., 1988; Brocchi et al., 2018; Johnson et
292 al., 2021). Domestic wood burning is an increasing trend in northern European cities (Chafe et al., 2015). Burning will generally
293 be in the winter during which, with short daylight hours and peak daytime OH often an order of magnitude lower than during
294 the summer, the reaction with NO$_3$ is likely to be the dominant fate of furan type compounds in such emissions, contributing
295 significantly to organic aerosol in urban areas (Kodros et al., 2020).

297 Berndt et al. (1997) identified the major first generation products of furan+NO_3 to be the unsaturated dicarbonyl, butenedial, and

298 2(3H)-furanone, with the NO_3 recycled back to NO_2. However, Tapia et al. (2011), and Joo et al. (2019) found that the major

299 products of the 3-methylfuran+NO_3 reaction predominantly retain the NO_3 functionality. In this case, furan+NO_3 oxidation

300 chemistry may be a significant sink for NOx, sequestering it in nitrate species, which might release it far from source on further

301 gas-phase oxidation, or, due to their low volatility, be taken up into aerosol (Joo et al. 2019).

313 **Table 5.** Atmospheric gas-phase lifetimes of the compounds reported herein based on typical mid-day OH concentrations of

314 5×10^6 molecules cm^{-3}, night-time NO_3 concentrations of 2×10^8 molecules cm^{-3}, day-time NO_3 concentrations of 1×10^7 molecules

315 cm^{-3}, and background O_3 concentrations of 40 ppbv (1×10^{12} molecules cm^{-3}).

Compound	$\tau_{NO3\ (night)}$	$\tau_{NO3\ (day)}$	$\tau_{OH\ (day)}$	τ_{O3}	$\tau_{total\ (day)}$
2,5-dimethylfuran	0.82 min	16 min	26 min [a]	40 min [b]	8 min
2-methylfuran	3.7 min	74 min	48 min [a]	-	28 min
furan	56 min	19 hours	83 min [a]	116 hours [c]	77 min
pyrrole	1.2 min	24 min	28 min [d]	18 hours [d]	13 mins
furfural	15 hours	13 days	95 min [e]	-	94 min
α-angelicalactone	28 min	9.3 hours	48 min [f]	3.5 hours [g]	37 mins
γ-crotonolactone	> 1.1 year	> 22 years	14 hours [h]	173 years	14 hours

316 [a] Matsumoto (2011); [b] Dillon et al. (2012); [c] Atkinson et al. (1983); [d] Atkinson et al. (1984); [e] Bierbach et al. (1995); [f] Bierbach

317 et al. (1994); [g] estimated (Bierbach et al., 1994); [h] Ausmeel et al. (2017)

318

319 **5 Conclusions**

320 Rate coefficients are recommended for reaction of seven furan type VOCs with NO_3 at 298 K and 760 Torr, based on a series of

321 relative rate experiments. These new recommendations highlight the importance of NO_3 chemistry to the removal of furans, and

322 other similar VOCs, under atmospheric conditions. The measured rate coefficients suggest that for the three furans reported here,

323 as well as for pyrrole and α-angelicalactone, reaction with NO_3 is likely to be their dominant night-time sink. For the alkyl furans

324 and pyrrole, reaction with NO_3 may also be a significant sink during the daytime. This work also extends the existing database
325 of VOC+NO_3 reactions, providing valuable reference values for future work.

326

327

328 *Data availability.* Further example plots and experiment information are provided in the supplement. All of the response-time
329 profiles from the FTIR are provided in .txt format at 10.5281/zenodo.5724967, and all of the raw FTIR output is provided in .csv
330 format at 10.5281/zenodo.5721518.

331

332 *Author contributions.* MJN performed the experiments with the technical support of YR and MRM and performed the data
333 treatment and interpretation. MJN wrote the paper. All co-authors revised the content of the original manuscript and approved
334 the final version of the paper.

335

336 *Competing interests.*
337 The authors declare that they have no conflict of interest.

338

339 *Special issue statement.* This article is part of the special issue "Simulation chambers as tools in atmospheric research
340 (AMT/ACP/GMD inter-journal SI)". It is not associated with a conference.

341

342 *Acknowledgements.*
343 This work is supported by the European Union's Horizon 2020 research and innovation program through the EUROCHAMP-
344 2020 Infrastructure Activity under grant agreement no. 730997, Labex Voltaire (ANR-10-LABX-100-01) and ANR (SEA_M
345 project, ANR-16-CE01-0013, program ANR-RGC 2016).

346

347 Financial support. This research has been supported by the European Commission Horizon 2020 Framework Programme (grant
348 no. EUROCHAMP-2020 (730997)) and the Agence Nationale de la Recherche (grants nos. ANR-10-LABX-100-01 and ANR-
349 16-CE01-0013)

350 **References**

351 Ahern, A. T., Robinson, E. S., Tkacik, D. S., Saleh, R., Hatch, L. E., Barsanti, K. C., Stockwell, C. E., Yokelson, R. J., Presto,
352 A. A., Robinson, A. L., Sullivan, R. C., and Donahue, N. M.: Production of Secondary Organic Aerosol During Aging of Biomass
353 Burning Smoke From Fresh Fuels and Its Relationship to VOC Precursors, J. Geophys. Res.-Atmos., 124, 3583–3606, 2019.

354

355 Akherati, A., He, Y., Coggon, M. M., Koss, A. R., Hodshire, A. L., Sekimoto, K., Warneke, C., de Gouw, J., Yee, L., Seinfeld,
356 J. H., Onasch, T. B., Herndon, S. C., Knighton, W. B., Cappa, C. D., Kleeman, M. J., Lim, C. Y., Kroll, J. H., Pierce, J. R., and
357 Jathar, S. H.: Oxygenated Aromatic Compounds are Important Precursors of Secondary Organic Aerosol in Biomass Burning
358 Emissions, Environ. Sci. Technol., 54, 8568–8579, https://doi.org/10.1021/acs.est.0c01345, 2020.

359

360 Andreae, M. O., Browell, E. V., Garstang, M,. Gregory, G. L., Harriss, R. C., Hill, G. F., Jacob, D. J., Pereira, C., Sachse, G.
361 W., Setzer, A. W., Silva Dias, P. L., Talbot, R. W., Torres, A. L., and Wofsy, S. C.: Biomass-burning emissions and associated
362 haze layers over Amazonia, J. Geophys. Res.-Atmos, 93, 1509-1527, 1988.

363

364 Andreae, M. O.: Emission of trace gases and aerosols from biomass burning – an updated assessment, Atmos. Chem. Phys., 19,
365 8523–8546, https://doi.org/10.5194/acp-19-8523-2019, 2019.
366

367 Aschmann, S. M., Nishino, N., Arey J., and Atkinson, R.: Products of the OH radical-initiated reactions of furan, 2- and 3-
368 methylfuran, and 2,3- and 2,5-dimethylfuran in the presence of NO, J. Phys. Chem. A, 118, 457-466, 2014.
369

370 Atkinson, R., Aschmann, S. M., and Carter, W. P. L.: Kinetics of the reactions of O3 and OH radicals with furan and thiophene
371 at 298 +/- 2 K, Int. J. Chem. Kinet., 15, 51-61, 1983.
372

373 Atkinson, R., Aschmann, S. M., Winer, A. M., and Carter, W. P. L.: Rate Constants for the Gas Phase Reactions of OH Radicals
374 and O_3 with Pyrrole at 295 +/- 1 K and Atmospheric Pressure, Atmos. Environ., 18, 2105-2107, 1984.
375

376 Atkinson, R., Aschmann, S. M., Winer, A. M., and Pitts, J. N.: Gas-phase reactions of NO_2 with alkenes and dialkenes, Int. J.
377 Chem. Kinet., 16, 697-706, 1984.
378

379 Atkinson, R., Aschmann, S. M., Winer, A. M., and Carter, W. P. L.: Rate Constants for the Gas Phase Reactions of NO_3 Radicals
380 with Furan, Thiophene and Pyrrole at 295 +/- 1 K and Atmospheric Pressure, Environ. Sci. Technol., 19, 87-90, 1985.
381

382 Ausmeel, S., Andersen, C., Nielsen, O. J., Østerstrøm, F. F., Johnson, M. S., and Nilsson, E. J. K.: Reactions of Three Lactones
383 with Cl, OD, and O_3: Atmospheric Impact and Trends in Furan Reactivity, J. Phys. Chem. A, 121, 4123-4131, 2017.
384

385 Barnes, I., Bastian, V., Becker, K. H., and Tong, Z.: Kinetics and products of the reactions of nitrate radical with monoalkenes,
386 dialkenes, and monoterpenes, J. Phys. Chem*., 94, 2413–2419, 1990.
387

388 Bernard, F., Cazaunau, M., Mu, Y., Wang, X., Daële, V,. Chen, J., and Mellouki, A.: Reaction of NO_2 with conjugated alkenes,
389 J. Phys. Chem. A, 117, 14132-14140, 2013.
390

391 Berndt, T., Böge, O., and Rolle, W.: Products of the Gas-Phase Reactions of NO_3 Radicals with Furan and Tetramethylfuran,
392 Environ. Sci. Technol., 31, 1157–1162, 1997.
393

394 Bierbach, A., Barnes, I., Becker, K. H., and Wiesen, E.: Atmospheric Chemistry of Unsaturated Carbonyls: Butenedial, 4-Oxo-
395 2-pentenal, 3-Hexene-2,5-dione, Maleic Anhydride, 3H-Furan-2-one, and 5-Methyl-3H-furan-2-one, Environ. Sci. Technol., 28,
396 715-729, 1994.
397

398 Bierbach, A., Barnes, I., and Becker, K. H.: Product and kinetic study of the OH-initiated gas-phase oxidation of furan, 2-
399 methylfuran and furanaldehydes at ≈ 300 K, Atmos. Environ., 29, 2651−2660, 1995.
400

401 Binder, J. B., and Raines, R. T.: Simple Chemical Transformation of Lignocellulosic Biomass into Furans for Fuels and
402 Chemicals. J. Am. Chem. Soc., 131, 1979−1985, 2009.
403

404 Bloss, C., Wagner, V., Jenkin, M. E., Volkamer, R., Bloss, W. J., Lee, J. D., Heard, D. E., Wirtz, K., Martin-Reviejo, M., Rea,
405 G., Wenger, J. C., and Pilling, M. J.: Development of a detailed chemical mechanism (MCMv3.1) for the atmospheric oxidation
406 of aromatic hydrocarbons, Atmos. Chem. Phys., 5, 641–664, https://doi.org/10.5194/acp-5-641-2005, 2005.
407

408 Brocchi, V., Krysztofiak, G., Catoire, V., Guth, J., Marécal, V., Zbinden, R., El Amraoui, L., Dulac, F., and Ricaud, P.:
409 Intercontinental transport of biomass burning pollutants over the Mediterranean Basin during the summer 2014 ChArMEx-
410 GLAM airborne campaign, Atmos. Chem. Phys., 18, pp. 6887-6906, 2018.
411

412 Brown, S., and Stutz, J.: Nighttime radical observations and chemistry, Chem. Soc. Rev., 41, 6405-6447, 2012.

415

416 Cabañas, B., Baeza, M. T., Salgado, S., Martín, P., Taccone, R., and Martínez, E.: Oxidation of heterocycles in the atmosphere:
417 Kinetic study of their reactions with NO_3 radical, J. Phys. Chem. A, 108, 10818-10823, 2004.

418

419 Chafe, Z., Brauer, M., Héroux, M. –E., Klimont, Z., Lanki, T., Salonen, R. O., and Smith, K. R.: Residential heating with wood
420 and coal: health impacts and policy options in Europe and North America, WHO Regional Office for
421 Europe. https://apps.who.int/iris/handle/10665/153671, 2015.

422

423 Coggon, M. M., Lim, C. Y., Koss, A. R., Sekimoto, K., Yuan, B., Gilman, J. B., Hagan, D. H., Selimovic, V., Zarzana, K. J.,
424 Brown, S. S., M Roberts, J., Müller, M., Yokelson, R., Wisthaler, A., Krechmer, J. E., Jimenez, J. L., Cappa, C., Kroll, J. H., De
425 Gouw, J. and Warneke, C.: OH chemistry of non-methane organic gases (NMOGs) emitted from laboratory and ambient biomass
426 burning smoke: Evaluating the influence of furans and oxygenated aromatics on ozone and secondary NMOG formation, Atmos.
427 Chem. Phys., 19, 14875–14899, doi:10.5194/acp-19-14875-2019, 2019.

428

429 Colmenar, I., Cabañas, B., Martínez, E., Salgado, M. S., and Martín, P.: Atmospheric fate of a series of furanaldehydes by their
430 NO_3 reactions, Atmos. Environ., 54, 177-184, 2012.

431

432 Decker, Z. C. J., Zarzana, K. J., Coggon, M., Min, K.-E., Pollack, I., Ryerson, T. B., Peischl, J., Edwards, P., Dubé, W. P.,
433 Markovic, M. Z., Roberts, J. M., Veres, P. R., Graus, M., Warneke, C., de Gouw, J., Hatch, L. E., Barsanti, K. C. and Brown, S.
434 S.: Nighttime Chemical Transformation in Biomass Burning Plumes: A Box Model Analysis Initialized with Aircraft
435 Observations, Environ. Sci. Technol., 53, 2529–2538, doi:10.1021/acs.est.8b05359, 2019.

436

437 Dillon, T. J., Tucceri, M. E., Dulitz, K., Horowitz, A., Vereecken, L., and Crowley, J.: Reaction of Hydroxyl Radicals with
438 C4H5N (Pyrrole): Temperature and Pressure Dependent Rate Coefficients, J. Phys. Chem. A, 116, 6051-6058, 2012.

439

440 Harvey B. J.: Human-caused climate change is now a key driver of forest fire activity in the western United States, Proc. Natl.
441 Acad. Sci., 113, 11649-11650, 2016.

442

443 Hartikainen, A., Yli-Pirilä, P., Tiitta, P., Leskinen, A., Kortelainen, M., Orasche, J., Schnelle-Kreis, J., Lehtinen, K.,
444 Zimmermann, R., Jokiniemi, J., and Sippula, O.: Volatile Organic Compounds from Logwood Combustion: Emissions and
445 Transformation under Dark and Photochemical Aging Conditions in a Smog Chamber, Environ. Sci. Technol., 52, 4979-4988,
446 2018.

447

448 Hatch, L. E., Luo, W., Pankow, J. F., Yokelson, R. J., Stockwell, C. E., and Barsanti, K. C.: Identification and quantification of
449 gaseous organic compounds emitted from biomass burning using two-dimensional gas chromatography–time-of-flight mass
450 spectrometry, Atmos. Chem. Phys., 15, 1865–1899, https://doi.org/10.5194/acp-15-1865-2015, 2015.

451

452 Hatch, L. E., Yokelson, R. J., Stockwell, C. E., Veres, P. R., Simpson, I. J., Blake, D. R., Orlando, J. J., and Barsanti, K. C.:
453 Multi-instrument comparison and compilation of non-methane organic gas emissions from biomass burning and implications for
454 smoke-derived secondary organic aerosol precursors, Atmos. Chem. Phys., 17, 1471–1489, 2017.

455

456 Hjorth, J., Lohse, C., Nielsen, C. J., Skov, H., and Restelli, G.: Products and mechanism of the gas-phase reaction between
457 NO_3 and a series of alkenes, J. Phys. Chem., 94, 7494–7500, 1990.

458

459 Jenkin, M. E., Saunders, S. M., and Pilling, M. J.: The tropospheric degradation of volatile organic compounds: a protocol for
460 mechanism development, Atmos. Environ., 31, 81–104, https://doi.org/10.1016/S1352-2310(96)00105-7, 1997 (data available
461 at: http://mcm.york.ac.uk, last access: 12 August 2021).

462

Deleted: [2]

465 Jenkin, M. E., Valorso, R., Aumont, B., Newland, M. J., and Rickard, A. R.: Estimation of rate coefficients for the reactions of
466 O_3 with unsaturated organic compounds for use in automated mechanism construction, Atmos. Chem. Phys., 20, 12921–12937,
467 https://doi.org/10.5194/acp-20-12921-2020, 2020.
468
469 Johnson, M. S., Strawbridge, K., Knowland, K. E., Keller, C., and Travis, M.: Long-range transport of Siberian biomass burning
470 emissions to North America during FIREX-AQ, Atmos. Environ., 252, 118241, 2021
471
472 Jolly, W. M., Cochrane, M. A., Freeborn, P. H., Holden, Z. A., Brown, T. J., Williamson, G. J., and Bowman, D. M. J. S.:
473 Climate-induced variations in global wildfire danger from 1979 to 2013, Nat. Commun., 6, 7537, 2015.
474
475 Kerdouci, J., Picquet-Varrault, B., and Doussin, J. –F.: Structure activity relationship for the gas-phase reactions of NO_3 radical
476 with organic compounds: Update and extension to aldehydes, Atmos. Environ., 84, 363-372, 2014.
477
478 Kind, I., Berndt, T., Böge, O., and Rolle, W.: Gas-phase rate constants for the reaction of NO_3 radicals with furan and methyl-
479 substituted furans, Chem. Phys. Lett., 256, 679-683, 1996.
480
481 Kodros, J., Papanastasiou, D., Paglione, M., Masiol, M. and Squizzato, S.: Rapid dark aging of biomass burning as an overlooked
482 source of oxidized organic aerosol, 117, 33028-33033, 2020.
483
484 Koss, A. R., Sekimoto, K., Gilman, J. B., Selimovic, V., Coggon, M. M., Zarzana, K. J., Yuan, B., Lerner, B. M., Brown, S. S.,
485 Jimenez, J. L., Krechmer, J., Roberts, J. M., Warneke, C., Yokelson, R. J., and de Gouw, J.: Non-methane organic gas emissions
486 from biomass burning: identification, quantification, and emission factors from PTR-ToF during the FIREX 2016 laboratory
487 experiment, Atmos. Chem. Phys., 18, 3299–3319, https://doi.org/10.5194/acp-18-3299-2018, 2018.
488
489 Krikken, F., Lehner, F., Haustein, K., Drobyshev, I., and van Oldenborgh, G. J.: Attribution of the role of climate change in the
490 forest fires in Sweden 2018, Nat. Hazards Earth Syst. Sci., 21, 2169–2179, https://doi.org/10.5194/nhess-21-2169-2021, 2021.
491
492 Kurtén, T., Møller, K. H., Nguyen, T. B., Schwantes, R. H., Misztal, P. K., Su, L., Wennberg, P. O., Fry J. L., and Kjaergaard,
493 H. G.: Alkoxy Radical Bond Scissions Explain the Anomalously Low Secondary Organic Aerosol and Organonitrate Yields
494 From alpha-Pinene + NO_3, J. Phys. Chem. Lett., 8, 2826–2834, 2017.
495
496 Kwok, E. S. C., and Atkinson, R.: Estimation of hydroxyl radical reaction rate constants for gas-phase organic compounds using
497 a structure-reactivity relationship: An update, Atmos. Environ., 29, 1685-1695, 10.1016/1352-2310(95)00069-b, 1995.
498
499 Lohmander, P.: Forest fire expansion under global warming conditions: Multivariate estimation, function properties, and
500 predictions for 29 countries, Central Asian Journal of Environmental Science and Technology Innovation, 5, 262-276, 2020.
501
502 Matsumoto, J.: Kinetics of the reactions of ozone with 2,5-dimethylfuran and its atmospheric implications, Chem. Lett., 40, 582-
503 583, 2011.
504
505 McGillen, M. R., Archibald, A. T., Carey, T., Leather, K. E., Shallcross, D. E., Wenger, J. C., and Percival, C. J.: Structure-
506 activity relationship (SAR) for the prediction of gas-phase ozonolysis rate coefficients: an extension towards heteroatomic
507 unsaturated species, Phys. Chem. Chem. Phys., 13, 2842-2849, 2011.
508
509 McGillen, M. R., Carter, W. P. L., Mellouki, A., Orlando, J. J., Picquet-Varrault, B., and Wallington, T. J.: Database for the
510 kinetics of the gas-phase atmospheric reactions of organic compounds, Earth Syst. Sci. Data, 12, 1203–1216,
511 https://doi.org/10.5194/essd-12-1203-2020, 2020.
512

513 Newland, M. J., Rea, G. J., Thüner, L. P., Henderson, A. P., Golding, B. T., Rickard, A. R., Barnes, I., and Wenger, J.:
514 Photochemistry of 2-butenedial and 4-oxo-2-pentenal under atmospheric boundary layer conditions, Phys. Chem. Chem. Phys.,
515 21, 1160-1171, 2019.
516
517 Novelli, A., Cho, C., Fuchs, H., Hofzumahaus, A., Rohrer, F., Tillmann, R., Kiendler-Scharr, A., Wahner, A., and Vereecken,
518 L.: Experimental and theoretical study on the impact of a nitrate group on the chemistry of alkoxy radicals, 23, 5474-5495, 2021.
519
520 Parrish, D. D., Lamarque, J. F., Naik, V., Horowitz, L., Shindell, D. T., Staehelin, J., Derwent, R., Cooper, O. R., Tanimoto, H.,
521 Volz-Thomas, A., Gilge, S., Scheel, H. E., Steinbacher, M. and Fröhlich, M.: Long-term changes in lower tropospheric baseline
522 ozone concentrations: Comparing chemistry-climate models and observations at northern midlatitudes, J. Geophys. Res., 119,
523 5719–5736, doi:10.1002/2013JD021435, 2014.
524
525 Ródenas, M: software for analysis of Infrared spectra. EUROCHAMP-2020 project, 2018. Available at
526 https://data.eurochamp.org/anasoft
527
528 Roman-Leshkov, Y., Barrett, C. J., Liu, Z. Y., and Dumesic, J. A.: Production of Dimethylfuran for Liquid Fuels from Biomass-
529 derived Carbohydrates, Nature, 447, 982−985, 2007.
530
531 Smith, D. F., McIver, C. D., and Kleindienst, T. E.: Primary product distribution from the reaction of hydroxyl radicals with
532 toluene at ppb NOx mixing ratios, J. Atmos. Chem., 30, 209–228, 1998.
533
534 Smith, D. F., Kleindienst, T. E., and McIver, C. D.: Primary Product Distributions from the Reaction of OH with m-, p-Xylene,
535 1,2,4- and 1,3,5-Trimethylbenzene, J. Atmos. Chem., 34, 339–364, 1999.
536
537 Sommariva, R., Cox, S., Martin, C., Borońska, K., Young, J., Jimack, P. K., Pilling, M. J., Matthaios, V. N., Nelson, B. S.,
538 Newland, M. J., Panagi, M., Bloss, W. J., Monks, P. S., and Rickard, A. R.: AtChem (version 1), an open-source box model for
539 the Master Chemical Mechanism, Geosci. Model Dev., 13, 169–183, https://doi.org/10.5194/gmd-13-169-2020, 2020.
540
541 Stewart, G. J., Acton, W. J. F., Nelson, B. S., Vaughan, A. R., Hopkins, J. R., Arya, R., Mondal, A., Jangirh, R., Ahlawat, S.,
542 Yadav, L., Sharma, S. K., Dunmore, R. E., Yunus, S. S. M., Hewitt, C. N., Nemitz, E., Mullinger, N., Gadi, R., Sahu, L. K.,
543 Tripathi, N., Rickard, A. R., Lee, J. D., Mandal, T. K., and Hamilton, J. F.: Emissions of non-methane volatile organic compounds
544 from combustion of domestic fuels in Delhi, India, Atmos. Chem. Phys., 21, 2383–2406, https://doi.org/10.5194/acp-21-2383-
545 2021, 2021a.
546
547 Stewart, G. J., Nelson, B. S., Acton, W. J. F., Vaughan, A. R., Hopkins, J. R., Yunus, S. S. M., Hewitt, C. N., Nemitz, E.,
548 Mullinger, N., Gadi, R., Rickard, A. R., Lee, J. D., Mandal, T. K., and Hamilton, J. F.: Comprehensive organic emission profiles,
549 secondary organic aerosol production potential, and OH reactivity of domestic fuel combustion in Delhi, India, Environ. Sci.:
550 Atmos., https://doi.org/10.1039/D0EA00009D, online first, 2021b.
551
552 Stone, D., Whalley, L., and Heard, D.: Tropospheric OH and HO_2 radicals: field measurements and model comparisons, Chem.
553 Soc. Rev., 41, 6348-6404, 2012.
554
555 Wang, J. J., Liu, X. H., Hu, B. C., Lu, G. Z., Wang, Y. Q.: Efficient Catalytic Conversion of Lignocellulosic Biomass into
556 Renewable Liquid Biofuels via Furan Derivatives. RSC Adv., 4, 31101− 31107, 2014.
557
558 Whelan, C. A., Eble, J. Mir, Z. S., Blitz, M. A., Seakins, P. W., Olzmann, M., and Stone D.: Kinetics of the Reactions of Hydroxyl
559 Radicals with Furan and Its Alkylated Derivatives 2-Methyl Furan and 2,5-Dimethyl Furan, *J. Phys. Chem. A*, 124, 7416–7426,
560 2020.
561

562 Wyche, K. P., Monks, P. S., Ellis, A. M., Cordell, R. L., Parker, A. E., Whyte, C., Metzger, A., Dommen, J., Duplissy, J., Prevot,
563 A. S. H., Baltensperger, U., Rickard, A. R., and Wulfert, F.: Gas phase precursors to anthropogenic secondary organic aerosol:
564 detailed observations of 1,3,5-trimethylbenzene photooxidation, Atmos. Chem. Phys., 9, 635–665, https://doi.org/10.5194/acp-
565 9-635-2009, 2009.
566
567 Yuan, Y., Zhao, X., Wang, S., and Wang, L: Atmospheric Oxidation of Furan and Methyl-Substituted Furans Initiated by
568 Hydroxyl Radicals, J. Phys. Chem. A, 121, 9306-9319, 2017.
569
570 Zhou, L., Ravishankara, A. R., Brown, S. S., Idir, M., Zarzana, K. J., Daële, V., and Mellouki, A.: Kinetics of the Reactions of
571 NO_3 Radical with Methacrylate Esters, J. Phys. Chem. A, 121, 4464-4474, 2017.

Berndt, T., Böge, O., Kind, I., and Rolle, W.: Reaction of NO_3 Radicals with 1,3-cyclohexadiene, α-terpinene, and α-phellandrene, Ber. Bunsenges. Phys. Chem, 100, 462–469, 1996.

Fouqueau, A., Cirtog, M., Cazaunau, M., Pangui, E., Doussin J. -F., and Picquet-Varrault, B.: A comparative and experimental study of the reactivity with nitrate radical of two terpenes: *α*-terpinene and *γ*-terpinene, Atmos. Chem. Phys., 20, 15167-15189, 2020.